RESEARCH ARTICLE

Prediction of cirrhosis using deep learning convolutional neural network model

Xiaodong Liu*

College of Pharmacy, Luohe Medical College, Luohe, Henan, China.

Received: February 20, 2025; **accepted:** June 11, 2025.

Cirrhosis is a common chronic liver disease, and early diagnosis is meaningful for delaying the course of the disease and improving the quality of patients' life. Traditional diagnostic methods for cirrhosis rely on imaging examinations, blood biochemical indicators, and pathological examinations. However, these methods often have certain limitations such as high costs, low accuracy in early diagnosis, and discomfort caused by invasive examinations. This study proposed a cirrhosis prediction system based on a deep learning convolutional neural network (CNN) optimized with advanced technologies of multi-level feature fusion, attention mechanisms, and residual connections. The proposed system integrated clinical data, imaging data, and biochemical indicators of patients, automatically extracted features, and performed classification prediction using the CNN model to achieve early diagnosis and risk assessment of cirrhosis. The results demonstrated that the CNN-based cirrhosis prediction system exhibited higher accuracy, stability, and reliability than that of traditional diagnostic methods. Particularly in the integration of multimodal data, the proposed system effectively enhanced prediction performance and significantly improved the early diagnosis rate of cirrhosis. Furthermore, the system offers personalized treatment and management recommendations to assist physicians in decision-making, thereby improving the precision of clinical treatment. This study presented a novel technical solution for the early diagnosis of cirrhosis with significant clinical application prospects.

Keywords: deep learning; convolutional neural network; cirrhosis; early diagnosis; risk assessment; clinical application.

***Corresponding author:** Xiaodong Liu, College of Pharmacy, Luohe Medical College, Luohe 462300, Henan, China. Email: liuxiaodong0411@126.com.

Introduction

Cirrhosis is the end-stage manifestation of widespread liver injury and fibrosis caused by various chronic liver diseases and characterized by high mortality and morbidity rates. According to the World Health Organization (WHO), cirrhosis has become one of the major public health challenges globally, particularly in the Asian region, where its incidence and mortality rates remain persistently high [1]. Cirrhosis not only directly leads to severe consequences such as liver failure and liver cancer but also imposes a substantial long-term socio-economic burden [2, 3]. The early detection and intervention in cirrhosis are significant in improving patient prognosis, reducing mortality, and alleviating the socio-economic burden. Currently, the diagnosis of cirrhosis primarily relies on imaging studies, biochemical blood markers, and pathological examinations. Common imaging techniques including ultrasound, computed tomography (CT), and magnetic resonance imaging (MRI) can assess liver structure and function but exhibit

limited sensitivity in the early stages of cirrhosis [4]. Biochemical markers including liver function tests and liver fibrosis scores such as aspartate aminotransferase to platelet ratio index (APRI) and fibrosis-4 score (FIB-4) can provide certain insights although they are susceptible to interference from various factors [5]. While liver biopsy is considered the gold standard for definitive diagnosis [6], its invasiveness and associated patient discomfort make it impractical as a routine screening method. In recent years, liver elastography techniques such as transient elastography and magnetic resonance elastography have gained widespread attention due to their non-invasiveness and ease of use [7, 8]. However, those traditional diagnostic methods still face limitations, which include high costs, complex procedures, and insufficient sensitivity to detect early subtle changes.

With the advancement of computer hardware performance, artificial intelligence (AI) technologies, particularly deep learning methods, have made significant progress in the field of medical image analysis [9]. Deep learning is a learning approach that simulates the neural network mechanism of the human brain, enabling automatic feature extraction through training on large datasets, and performing tasks such as classification, regression, and prediction. Convolutional neural networks (CNN), a typical architecture in deep learning, automatically extracts features from input data through convolutional layers and has been widely applied in image processing, speech recognition, and natural language processing [10]. In the field of medical imaging, CNNs can automatically extract texture, shape, and edge features from image data of CT, MRI, and ultrasound, significantly improving diagnostic accuracy in interesting areas such as ovarian tumors [11], colon cancer [12], and medical prediction systems [13]. There has been an increasing number of studies on CNN models for liver disease prediction with preliminary progress recently, particularly in the areas of liver image analysis, blood biochemical markers, and the integration of clinical data [14]. Previous research has demonstrated that deep learning models based on CT or MRI images can achieve high-precision detection of liver lesions and show promise in identifying early manifestations of cirrhosis [15, 16]. Additionally, combining radiomics with deep learning techniques by extracting many high-dimensional imaging features can reveal subtle changes in liver fibrosis development and predict the progression of cirrhosis [17]. In animal studies, research has also confirmed that CNNs can effectively identify fibrotic regions in mouse liver tissue, providing potential for translational medical applications [18]. Meanwhile, some researchers have proposed multimodal deep learning models that combine blood biochemical markers with imaging data, which can further enhance the predictive performance for liver fibrosis and cirrhosis [19]. However, there is still a limited amount of CNN research specifically targeting early prediction of cirrhosis. Despite the progress made in existing studies, predicting cirrhosis using deep learning still faces numerous challenges, which include the diversity and quality control issues of imaging and clinical data that require optimization of data collection, annotation, management processes and the exploration of how to implement the model's application in real-world clinical settings including the establishment of multi-center, large-scale datasets, improving model interpretability, and developing mechanisms for collaboration between physicians and AI. In addition, the sensitivity and specificity of traditional imaging and AI models need further improvement to better meet the demands of different clinical scenarios.

This research proposed a cirrhosis prediction method based on an improved CNN model, aiming to combine image features and biomarker data to propose a more accurate cirrhosis prediction model. Compared to traditional CNN, this study optimized its architecture by employing innovative technologies of multi-level feature fusion, attention mechanisms, and residual connections, enhancing the model's predictive accuracy and generalization capabilities. The proposed CNN-based early

prediction model for cirrhosis would hold the potential to overcome the limitations of traditional methods and improve the efficiency of early screening for cirrhosis. The findings of this research could provide valuable reference for the subsequent application of deep learning in the early diagnosis of other chronic liver diseases, fostering a deeper integration of medical artificial intelligence with clinical practice and was expected to have a positive impact on reducing the mortality rate of cirrhosis patients and improving public health standards.

Materials and methods

Basic CNN model framework

The basic CNN structure consists of multiple convolutional layers, pooling layers, and fully connected layers [20]. The convolution operation was the core of CNN as below.

$$Y_{i,j,k} = \sum_{m=1}^{M} \sum_{n=1}^{N} X_i + m, j + n \cdot W_{m,n,k} + b_k \quad (1)$$

where X was the input image with size $H \times W \times C$. W was the convolution kernel (filter) with size $M \times N \times C$. Y was the output of the convolutional layer with size $(H - M + 1) \times (W - N + 1) \times K$. K was the number of convolution kernels. b_k was the bias of the k^{th} convolution kernel. m and n in the convolution operation were the dimensional indexes of the convolution kernel, controlling the sliding window of the convolution kernel on the input image. With this convolution operation, the convolution kernel slid over the input image with a step size of 1, and the weighted sum of local regions computed by dot multiplication would produce new feature maps. As the number of convolutional layers increased, the model could gradually extract more complex semantic information from local features. The pooling operation typically follows the convolutional layers to reduce the size of the feature map while retaining essential feature information. The most used pooling operations are max pooling and average pooling. It was assumed that the size of the input feature map was $H \times W \times C$. The pooling operation usually used a 2 × 2 pooling window and step size of 2. The pooled feature map size was $\frac{H}{2} \times \frac{W}{2} \times C$. The pooling operation could reduce the amount of computation and prevent overfitting with the equation below.

$$Y_{i,j,k} = \max(X_{2i,2j,k}, X_{2i+1,2j,k}, X_{2i,2j+1,k}, X_{2i+1,2j+1,k}) \quad (2)$$

where the maximum pooling (Max pooling) operation was used to output the maximum value within each pooling window. After passing through multiple convolutional and pooling layers, the output feature map was flattened and fed into the fully connected layer. The fully connected layer performed a linear transformation using a set of weight matrices to map the feature map into the prediction space for classification or regression tasks. If the input features to the fully connected layer were $F_{flatten}$ (size $N \times 1$), the output F_{output} of the fully connected layer was as follows.

$$Foutput = W_{fc} F_{flatten} + b_{fc} \quad (3)$$

where W_{fc} was the weight matrix of the fully connected layer with size $N_{fc} \times N$. b_{fc} was the bias term with size $N_{fc} \times 1$. F_{output} was the output of the fully connected layer. At the last layer of the CNN, an activation function such as Softmax or Sigmoid was used to output the prediction result. For binary classification problems, the output layer could be a Sigmoid activation function as follows.

$$P_{(cirrhosis)} = \sigma(W_{out} F_{fusion} + b_{out}) \quad (4)$$

where σ was the Sigmoid function. W_{out} and b_{out} were the weights and biases of the output layer. For multi-classification problems, the Softmax activation function was usually used in the output layer as below.

$$P_{(category_i)} = \frac{exp(W_{out,i} \cdot F_{fusion} + b_{out,i})}{\sum_j exp(W_{out,j} \cdot F_{fusion} + b_{out,j})} \quad (5)$$

The Softmax function was used to calculate the probabilities for each class with the output being the predicted probabilities for each class.

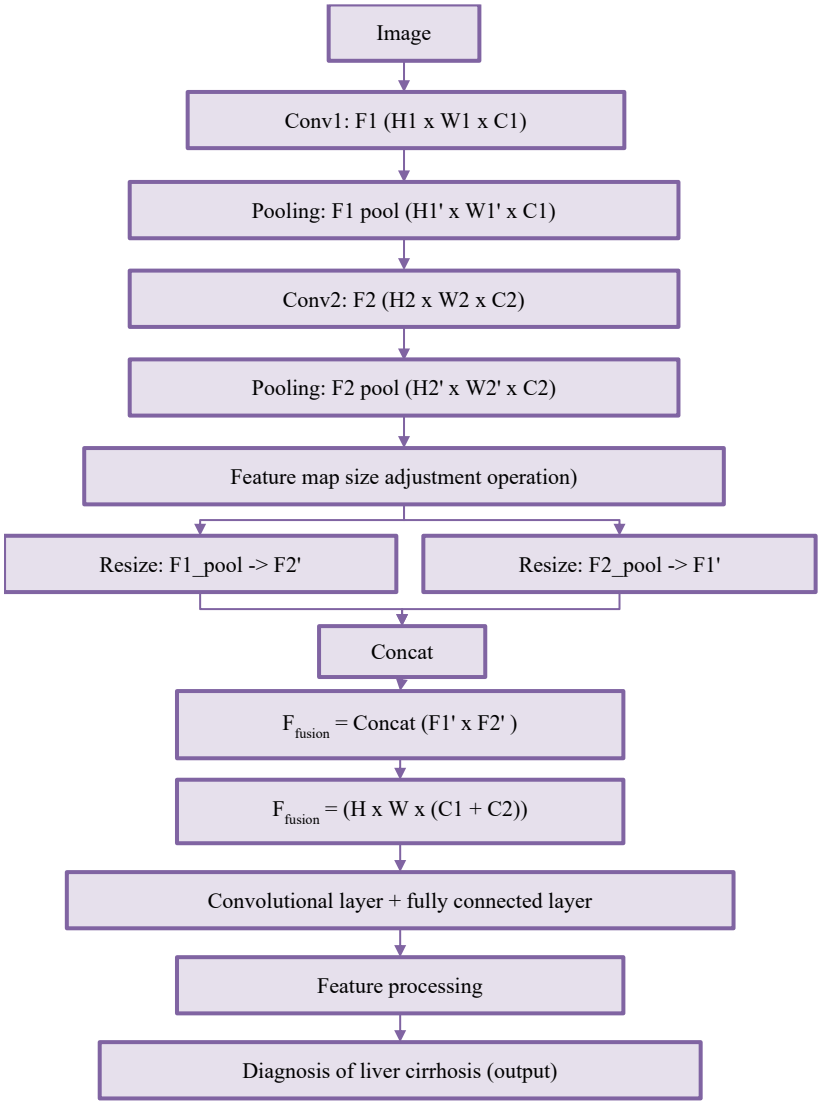

Figure 1. Structural diagram of multi-level feature fusion.

Model improvements

(1) Multi-level feature fusion

To fully exploit feature information at different scales, this research proposed a multi-level feature fusion strategy, which enhanced the model's multi-level understanding of cirrhosis images by combining features from both shallow and deep convolutional layers, thereby improving the accuracy of cirrhosis diagnosis. Specifically, features from intermediate layers of the convolutional network were fused to integrate low-level and high-level semantic information, which enhanced the network's representational capacity for different regions of the image, particularly for the subtle features of complex diseases like cirrhosis (Figure 1). It was supposed that there were two convolutional layers with output feature maps $F_1(H_2 \times W_2 \times C_{21})$ and $F_2(H \times W \times C)$ from the shallow like the second convolutional layer and deep such as the fourth convolutional layer of the network, respectively. These feature maps size might be different and must be processed. The resize operation was used to adjust the feature map to the same height H_2 and width W_2 by bilinear interpolation with the specific process shown below.

$$F_{fusion} = Concat(Resize(F_1, H_2, W_2), Resize(F_2, H_1, W_1)) \quad (6)$$

The resize operation refers to the resizing of feature maps to fit the target dimensions [21]. The interpolation method could be bilinear interpolation to ensure that the resized image would not lose too much detail. The Concat operation indicated that the two feature maps, after resizing, were concatenated along the channel dimension *i.e.* the third dimension [22]. Through such feature fusion, shallow and deep features were combined to form a fused feature map F_{fusion} that contained rich semantic information.

(2) Self-attention mechanism

The self-attention mechanism was designed to calculate attention weights for each image location, allowing the model to adaptively focus on key information areas in the input image and ignore irrelevant parts [23]. By incorporating the self-attention mechanism, CNN could more effectively model the image features of cirrhosis, particularly when identifying subtle changes and abnormal areas such as lesions or hardened regions in the liver. The key idea of the self-attention mechanism was to calculate the attention weights of each position with respect to other positions based on the relationship between the query, key, and value, thereby generating a weighted feature map. The self-attention mechanism was calculated using the following equations.

$$A_{ij} = \frac{\exp(Q_i \cdot K_j)}{\sum_{k=1}^{N} \exp(Q_i \cdot K_k)} \quad (7)$$

$$V_i^{new} = \sum_{j=1}^{N} A_{ij} V_j \quad (8)$$

where Q_i *and* K_j were the query and key vectors from the input features, respectively. V_j was the value vector, which represented the information of each position. A_{ij} was the attention weight of position *i* to position *j*. Based on weighting and calculating attention weight, the new feature map V_i^{new} was obtained, which contained more information about cirrhosis key areas.

(3) Residual connections

In deep neural networks, as the number of layers increases, the model may encounter the problem of vanishing or exploding gradients. These issues can hinder the optimization process during training, especially in deep networks. As the network depth increases, information from earlier layers may gradually be lost during transmission, making gradient propagation more difficult. To address these challenges and accelerate the training process, residual connections were introduced. Residual connections facilitated the flow of information by "skipping" certain layers and directly passing the input to subsequent layers. By providing shortcut paths, the vanishing and exploding of gradients were prevented. The residual connection core idea was that, at a certain layer of the network, the input X was not only processed by conventional convolution operations or other transformations $F(X, \{W_i\})$, but was also directly passed to the next layer of the network. The direct transfer formed the so-called "shortcut", allowing the input information to directly influence the final output without undergoing transformations from all layers as follows.

$$Y_{res} = X + F(X, \{W_i\}) \quad (9)$$

where *X* was the input feature. $F(X, \{W_i\})$ was the features obtained through network transformations such as convolutional operations and activation functions. This part was the "regular" operation of the network. Y_{res}, the output of the residual block, was equal to the sum of the input *X* and the transformed result of $F(X, \{W_i\})$. This structure introduced shortcut paths that directly added the input XXX to the transformed feature maps without the need for processing through all layers. This approach effectively mitigated the vanishing gradient problem and accelerated the training process.

(4) Comprehensive feature fusion and classification

To predict cirrhosis more accurately, this study combined imaging features with clinical data such as biochemical indicators related to liver

function and patient medical history for comprehensive analysis. Image data were extracted using CNN, while clinical data were processed by a multi-layer perceptron (MLP) model. Ultimately, the features from both sources were fused and passed into the classification layer for binary prediction. For image data processing and feature extraction, the image data X_{image} was input into the CNN for feature extraction. After multiple convolutional layers and pooling layers, the model obtained a feature map F_{image} containing high-level semantic information as follows.

Input: X_{image} (size $H \times W \times C_{image}$)

Output: F_{image} (size D_{image}, feature vector)

The CNN part extracted local and global features such as liver morphological changes and lesion areas related to cirrhosis in the image through a combination of convolution, pooling, and fully connected layers. For clinical data processing and feature extraction, clinical data X_{clin} contained the patient's biochemical indicators such as alanine aminotransferase (ALT), aspartate aminotransferase (AST), bilirubin, platelet count and other important physiological indicators. These data were numerical data, so feature extraction and nonlinear mapping through MLP with full connection layer were needed.

Input: X_{clin} (size N_{clin})

Output: F_{clin} (size D_{clin})

MLP model learned important features in clinical data through layer-by-layer linear transformations and nonlinear activation functions such as ReLU. The structure of MLP was expressed below.

$$F_{clin} = \sigma(W_{MLP}X_{clin} + b_{MLP}) \quad (10)$$

where W_{MLP} was the weight matrix of the MLP layer. b_{MLP} was the bias term. σ was the activation function. For feature fusion, the image features F_{image} and clinical data features F_{clin} were extracted from different sources, which contained different types of information. To enable the model to utilize the two parts of information at the same time, they were fused into a comprehensive feature vector F_{fusion} by concatenation operation as below.

$$F_{fusion} = Concat(F_{image}, F_{clin}) \quad (11)$$

After concatenation, the feature vector F_{fusion} contained the information of liver imaging features and clinical data features as shown below.

$$F_{fusion} \in \mathbb{R}^{D_{image}+D_{clin}} \quad (12)$$

For the classification layer and output, the fused feature vector F_{fusion} was passed to a fully connected layer, which was used to make a binary prediction as cirrhosis or non-cirrhosis based on the integrated features. The probability of cirrhosis, P (cirrhosis), was output through a Sigmoid activation function as the prediction result of the model. The output of the fully connected layer was expressed as below.

$$P_{(Cirrhosis)} = \sigma(W_{out}X_{fusion} + b_{out}) \quad (13)$$

where $W_{out} \in \mathbb{R}^{(D_{image}+D_{clin}) \times 1}$ was the weight matrix of the classification layer. b_{out} was the bias term of the classification layer. σ was the Sigmoid activation function as shown in equation (14).

$$\sigma_{(z)} = \frac{1}{1+\exp(-z)} \quad (14)$$

The Sigmoid function output a value between 0 and 1, representing the predicted probability after the integration of image and clinical data. Specifically, an output value close to 1 indicated that the patient was likely to have cirrhosis, while an output value close to 0 suggested that the patient was normal. To train the model, the binary cross-entropy loss function that measured

the difference between the output of the model and the true labels was shown below.

$$L = -[ylog(p) + (1-y)\log(1-p)] \quad (15)$$

where *y* was the true label as 0 for non-cirrhosis and 1 for cirrhosis. *p* was the predicted probability of the model output $P_{(Cirrhosis)}$. To minimize the loss function, the Adam optimization algorithm was used to update the parameters.

Data source

To evaluate the effectiveness of the CNN-based cirrhosis prediction model, this study utilized various medical datasets for validation and assessed the model's performance in early prediction of cirrhosis. The experimental data were collected from multiple hospitals and included clinical data of cirrhosis patients. The dataset comprised 500 patients including 250 cirrhosis patients and 250 non-cirrhosis patients. The dataset included several physiological and clinical characteristics of the patients including but not limited to gender, age, liver function markers such as ALT, AST, gamma-glutamyl transferase (GGT), total bilirubin, blood routine markers including white blood cell count (WBC) and hemoglobin concentration (Hb), abdominal imaging findings including liver echogenicity and spleen volume, and liver stiffness scores measured using transient elastography. All procedures of this study were approved by the Institutional Review Board (IRB) of Luohe Medical College (Luohe, Henan, China).

Evaluation metrics

This study first performed preprocessing on the imaging data by applying image augmentation techniques to standardize the CT/MRI images, ensuring data quality during model training. Additionally, a cross-validation method was employed to ensure the reliability of the experimental results with the dataset randomly divided into a training set (80%) and a testing set (20%). In evaluating the model's performance, this study utilized commonly used evaluation metrics including accuracy, sensitivity, specificity, F1 score, and precision shown in the equations below.

$$Accuracy = \frac{TP+TN}{TP+TN+FP+FN} \quad (16)$$

$$Sensitivity = \frac{TP}{TP+FN} \quad (17)$$

$$Specificity = \frac{TN}{TN+FP} \quad (18)$$

$$F1 = 2 \times \frac{Precision \times Sensitivity}{Precision+Sensitivity} \quad (19)$$

$$Precision = \frac{TP}{TP+FP} \quad (20)$$

where TP was true positive. TN was true negative. FP was false positive. FN was false negative.

Model performance validation and comparative analysis

To further validate the effectiveness of the proposed CNN model, this study compared it with several common traditional machine learning models including support vector machine (SVM), decision tree (DT), and random forest (RF). All traditional machine learning models were constructed and trained using the Scikit-learn toolkit (https://scikit-learn.org/). During the comparison process, the performance of each model based on metrics such as accuracy, sensitivity, specificity, and F1 score was evaluated to comprehensively assess the predictive capability of the deep learning model proposed in this research.

Sensitivity analysis of network architecture

To investigate the impact of different network layers on the results, a sensitivity analysis of the CNN model was further conducted. The focus of the analysis was on the influence of the convolutional layers and pooling layers on feature extraction and classification performance.

Development and testing method of the CNN-based cirrhosis prediction system

To validate the clinical application potential of the CNN-based cirrhosis prediction system, a

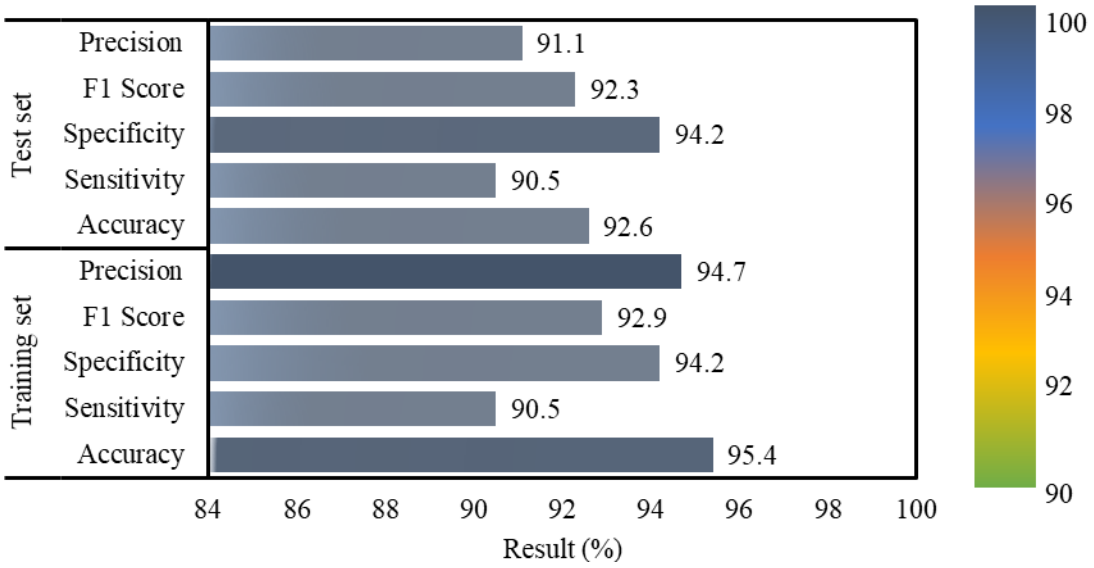

Figure 2. Evaluation indexes of the CNN-based cirrhosis prediction model (training set and test set).

complete prediction system was developed, encompassing modules for early cirrhosis prediction, clinical data analysis, and personalized treatment recommendations. The system testing design included two main modules. The early diagnosis and risk assessment module for cirrhosis input the patient's physiological, blood, and imaging data to predict their cirrhosis risk level, and the treatment and management recommendations module for cirrhosis patients generated personalized intervention and treatment plans based on the prediction results and individual patient characteristics. The system input data consisted of clinical data and imaging records collected from 2018 to 2023, covering patient information from multiple hospitals with a total sample size of 500 cases. During the testing process, the system performed a comprehensive analysis of various patient indicators including ALT and AST levels and imaging findings and classified predictions based on established high-risk standards. Additionally, the system provided personalized treatment and management recommendations for high-risk patients, considering their specific clinical indicators. In terms of regional analysis, the system integrated data from regions of Shanghai City, Guangdong Province, Jiangsu Province, Beijing City, Zhejiang Province, Sichuan Province, Shaanxi Province, Tianjin City, Shandong Province, Hubei Province, and Fujian Province to forecast future cirrhosis incidence trends across different areas and offer targeted screening and intervention suggestions.

Results and discussion

CNN-based cirrhosis prediction model

The CNN model developed in this study demonstrated excellent performance in the cirrhosis prediction task, achieving prediction accuracies of 95.4% and 92.6% on the training and testing datasets, respectively. The sensitivity and specificity were 90.5% and 94.2%, respectively, with an F1 score of 92.1%, indicating a strong ability to differentiate between cirrhosis and non-cirrhosis patients (Figure 2). This result was consistent with the previous study, where the deep convolutional neural network model for cirrhosis diagnosis achieved an accuracy of 96.8%, outperforming traditional methods such as SVM [24]. To comprehensively evaluate the performance of the proposed model, it was compared with three classical models of SVM, DT, and RF. The results showed that the CNN model outperformed the others across multiple metrics including accuracy, sensitivity, specificity,

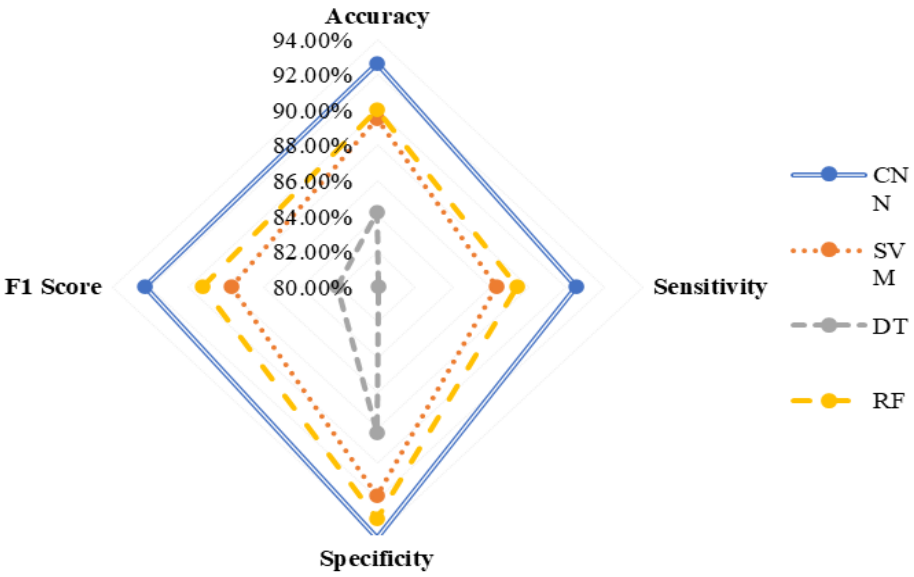

Figure 3. Comparative evaluation of different machine learning models in cirrhosis prediction.

Table 1. Sensitivity analysis of different network layers in the CNN model.

Network layer	Sensitivity	Specificity	F1 score
Original CNN model	90.50%	94.20%	92.30%
Remove convolutional layers	85.10%	90.40%	87.50%
Remove pooling layer	88.30%	91.70%	89.90%
Use only fully connected layer	82.20%	89.50%	85.80%
Optimize the convolutional and pooling layers	93.00%	95.10%	94.00%

and F1 score with a particularly significant advantage in F1 score (Figure 3). The previous study also indicated that, although RF performed well in several traditional tasks with an F1 score of 90.1%, it was still less accurate and stable than deep learning models in image recognition tasks [25]. This study further analyzed the contribution of different network layers in the CNN model to its performance. Sensitivity analysis revealed that both the convolutional and pooling layers were crucial for feature extraction. Removing the convolutional layer resulted in a 4.8% decrease in the F1 score, while removing the pooling layer led to a 2.4% decrease (Table 1). This observation supported the study by Byra *et al*. who evaluated fatty liver changes based on the Inception-ResNet-v2 architecture, where high performance was attributed to the deep feature learning capabilities of the multi-layer convolutional structure [26]. Brattain *et al*. suggested that, in liver fibrosis staging, the CNN model achieved an AUROC of 0.890 in assessing shear wave elastography image quality, significantly outperforming traditional stiffness indices with AUROC of 0.740 [27]. This further validated that deep networks excelled in feature representation in medical images compared to models based on shallow structures. Additionally, when compared with pre-trained networks like AlexNet-CNN, the results showed that the CNN model proposed in this study achieved higher accuracy in cirrhosis stage classification. Yu *et al*. confirmed that such models outperformed SVM and multi-class logistic regression (MLR) methods in metrics like AUROC, sensitivity, and specificity [28], which was highly consistent with the results of this study.

Table 2. Prediction results of high-risk cirrhosis patients.

Indicators	Total number of patients	Number of high-risk patients	Patients predicted to be high risk	Prediction accuracy (%)	Predictive sensitivity (%)	Predictive specificity (%)	F1 score (%)
ALT > 40 U/L	500	200	126	94.2	90.5	94.2	92.1
AST > 40 U/L	500	180	115	92.8	91.2	93.7	91.6
Imaging findings	500	150	95	91.3	89.7	92.4	90.5
Comprehensive judgment	500	180	113	94.2	90.5	94.2	92.6

Table 3. Treatment recommendations generated by the proposed system for 10 high-risk patients.

Patient ID	Age	Gender	ALT (U/L)	AST (U/L)	Imaging findings	Treatment recommendations
P001	55	Male	185	200	Significant liver fibrosis	Regular liver imaging examination, antiviral therapy, and improved diet
P002	63	Female	160	175	Liver structural changes	Increasing liver function monitoring, improving lifestyle, and avoiding alcohol and excessive fatigue
P003	58	Male	190	210	Liver sclerosis changes	Enhanced surveillance, antiviral therapy and weight control
P004	70	Female	210	220	Mild fibrosis	Regular early screening to optimize treatment
P005	50	Male	180	195	Irregular liver structure	Regular checkups, improving diet and lifestyle habits, and considering medication interventions
P006	62	Female	170	185	Tiny liver nodules	Continuing observation, antiviral therapy, and reducing alcohol consumption
P007	59	Male	150	165	Mild fatty liver	Healthy diet, exercise, and regular checkups
P008	54	Female	140	155	Normal liver structure	Maintaining a healthy lifestyle and getting regular screening
P009	68	Male	175	185	Calcified changes in the liver	Monitoring should be strengthened to avoid an increased burden on the liver
P010	61	Female	190	205	Progression of liver fibrosis	Antiviral therapy and regular liver function assessments

CNN model performance test and clinical application

By inputting data from 500 patients into the cirrhosis prediction system, the results showed that, for patients with ALT > 40 U/L, the proposed system achieved a prediction accuracy of 94.2%, sensitivity of 90.5%, specificity of 94.2%, and an F1 score of 92.1%. For patients with AST > 40 U/L, the prediction accuracy was 92.8%, sensitivity was 91.2%, specificity was 93.7%, and the F1 score was 91.6%. For patients with abnormal imaging findings, the prediction accuracy was 91.3%, and the overall prediction accuracy reached 94.2% (Table 2). These results were comparable to the performance of the DLRE system proposed by Wang *et al*., which achieved an AUROC of 0.970 in predicting F4 stage cirrhosis [29].

The proposed system of this study integrated individual patient characteristics and imaging findings to generate personalized treatment recommendations. For instance, for certain high-risk patients, the system would recommend frequent liver imaging exams, antiviral treatment, and lifestyle modifications. The results of treatment recommendations generated by the system for 10 high-risk cirrhosis patients included medications, regular check-ups, and dietary adjustments. Each patient's treatment plan was tailored based on their specific liver function markers, imaging changes, and lifestyle factors (Table 3).

Further regional analysis indicated that the system predicted an increase in the incidence of cirrhosis in the coming years, especially among the elderly population. In particular, the

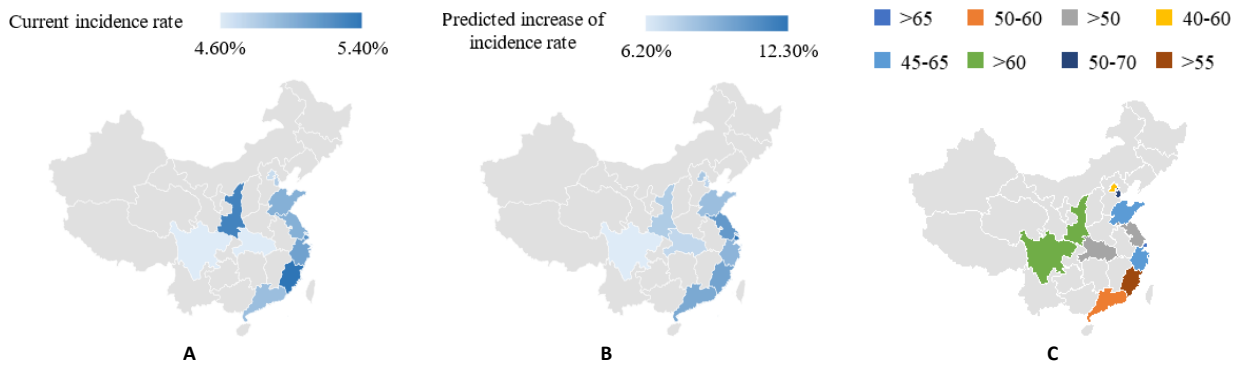

Figure 4. Prediction results of cirrhosis incidence trends in different regions of China. **A.** Current incidence rate of cirrhosis. **B.** Predicted increase in incidence rate. **C.** Key age groups.

incidence of cirrhosis in Shanghai was expected to continue to rise, especially among the elderly population over the age of 65. The system suggested strengthening early screening for elderly patients and increasing their focus in healthcare. The incidence of cirrhosis in Guangdong and Jiangsu provinces might increase in the next 3 - 5 years, especially among males aged 50 - 60. Therefore, the system recommended increasing the frequency of early screening in these areas and strengthening interventions for high-risk groups. The incidence of cirrhosis in Beijing and Zhejiang Province might slightly rise in the coming years, especially among people aged 40 – 60. The system suggested optimizing screening processes and enhancing health education to address this challenge. Sichuan and Shaanxi provinces showed a relatively stable trend in the incidence of cirrhosis, but there was a significant potential for increased incidence among the elderly population, and the system recommended increasing screening frequency for the elderly and focusing on lifestyle interventions. Tianjin, Shandong, Hubei, and Fujian showed a certain increasing trend in the incidence of cirrhosis, particularly among the middle-aged and elderly population, and the system suggested increasing health management for the middle-aged and elderly and increasing the frequency of related screenings (Figure 4). Based on the results, the incidence of cirrhosis demonstrated different increasing trends in high-incidence areas. The high-incidence areas such as Shanghai, Guangdong, and Jiangsu particularly need to strengthen screening and early intervention measures for high-risk groups. Areas like Sichuan and Shaanxi, although having a relatively stable incidence rate, have a significant potential for increased incidence among the elderly population, indicating that these areas should increase screening frequency for elderly patients.

This research proposed a CNN model-based cirrhosis prediction system, which possessed high predictive accuracy and strong clinical application value. The system was not only capable of assisting physicians in early diagnosis but also generating personalized treatment recommendations based on the clinical data and imaging presentations of patients. Furthermore, the system could conduct geographical analysis to provide support for public health decision-making. Overall, the deep learning CNN-based cirrhosis prediction system had a broad application prospect in clinical practice. The results demonstrated that the system exhibited good reliability, stability, and accuracy in early diagnosis of cirrhosis, personalized treatment, and public health management.

Acknowledgements

This work was supported by Henan Vocational Education Reform Research and Practice Project in 2017 (Grant No. 2017SJGLX593), The General Subject of Educational Science Planning of Henan

Provincial Department of Education (Grant No. 2023YB0551), The Scientific and Technological Research Project of Henan Science and Technology Department (Grant No. 162102310596).

References

1. Tan D, Chan KE, Wong ZY, Ng CH, Xiao J, Lim WH, *et al*. 2023. Global epidemiology of cirrhosis: changing etiological basis and comparable burden of nonalcoholic steatohepatitis between males and females. Dig Dis. 41(6):900-912.
2. Mohamed R, Yip C, Singh S. 2023. Understanding the knowledge, awareness, and attitudes of the public towards liver diseases in Malaysia. Eur J Gastroenterol Hepatol. 35(7):742-752.
3. Xie S, Yang L, Bi X, Deng W, Jiang T, Lin Y, *et al*. 2022. Cytokine profiles and CD8+ T cells in the occurrence of acute and chronic hepatitis B. Front Immunol. 13:1036612.
4. Cao L, Ling X, Yan J, Feng D, Dong Y, Xu Z, *et al*. 2024. Clinical and genetic study of ABCB4 gene-related cholestatic liver disease in China: Children and adults. Orphanet J Rare Dis. 19(1):157.
5. Di Ciaula A, Shanmugam H, Ribeiro R, Pina A, Andrade R, Bonfrate L, *et al*. 2023. Liver fat accumulation more than fibrosis causes early liver dynamic dysfunction in patients with non-alcoholic fatty liver disease. Eur J Intern Med. 107:52-59.
6. Chen Y, Wei M, Chen M, Wu C, Ding H, Pan X. 2024. A non-invasive diagnostic nomogram for CHB-related early cirrhosis: A prospective study. Sci Rep. 14(1):15343.
7. Mesropyan N, Kupczyk P, Isaak A, Endler C, Faron A, Dold L, *et al*. 2021. Synthetic extracellular volume fraction without hematocrit sampling for hepatic applications. Abdom Radiol (NY). 46(10):4637-4646.
8. Le Corvec M, Farrugia MA, Nguyen-Khac E, Régimbeau JM, Dharhri A, Chatelain D, *et al*. 2024. Blood-based MASH diagnostic in candidates for bariatric surgery using mid-infrared spectroscopy: A European multicenter prospective study. Sci Rep. 14(1):26452.
9. Mi J, Han X, Wang R, Ma R, Zhao D. 2022. Diagnostic accuracy of wireless capsule endoscopy in polyp recognition using deep learning: A meta-analysis. Int J Clin Pract. 2022:9338139.
10. Wang H, Liu X, Song L, Zhang Y, Rong X, Wang Y. 2024. Research on a train safety driving method based on fusion of an incremental clustering algorithm and lightweight shared convolution. Sensors (Basel). 24(15):4951.
11. Giourga M, Petropoulos I, Stavros S, Potiris A, Gerede A, Sapantzoglou I, *et al*. 2024. Enhancing ovarian tumor diagnosis: Performance of convolutional neural networks in classifying ovarian masses using ultrasound images. J Clin Med. 13(14):4123.
12. Gabralla LA, Hussien AM, AlMohimeed A, Saleh H, Alsekait DM, El-Sappagh S, *et al*. 2023. Automated diagnosis for colon cancer diseases using stacking transformer models and explainable artificial intelligence. Diagnostics (Basel). 13(18):2939.
13. Wang Y, Liu L, Wang C. 2023. Trends in using deep learning algorithms in biomedical prediction systems. Front Neurosci. 17:1256351.
14. Weng S, Hu D, Chen J, Yang Y, Peng D. 2023. Prediction of fatty liver disease in a Chinese population using machine-learning algorithms. Diagnostics (Basel). 13(6):1168.
15. Terradillos E, Saratxaga CL, Mattana S, Cicchi R, Pavone FS, Andraka N, *et al*. 2021. Analysis on the characterization of multiphoton microscopy images for malignant neoplastic colon lesion detection under deep learning methods. J Pathol Inform. 12:27.
16. Luetkens JA, Nowak S, Mesropyan N, Block W, Praktiknjo M, Chang J, *et al*. 2022. Deep learning supports the differentiation of alcoholic and other-than-alcoholic cirrhosis based on MRI. Sci Rep. 12(1):8297.
17. Park HJ, Park B, Lee SS. 2020. Radiomics and deep learning: hepatic applications. Korean J Radiol. 21(4):387-401.
18. Kim HJ, Baek EB, Hwang JH, Lim M, Jung WH, Bae MA, *et al*. 2023. Application of convolutional neural network for analyzing hepatic fibrosis in mice. J Toxicol Pathol. 36(1):21-30.
19. Wei W, Yang X. 2021. Utility of convolutional neural network-based algorithm in medical images for liver fibrosis assessment. Chin Med J (Engl). 134(18):2255-2257.
20. Shen Y, Wu J, Chen J, Zhang W, Yang X, Ma H. 2024. Quantitative detection of pipeline cracks based on ultrasonic guided waves and convolutional neural network. Sensors (Basel). 24(4):1204.
21. Liu T, Chen M, Duan Z, Cui A. 2024. Multi-focused image fusion algorithm based on multi-scale hybrid attention residual network. PLoS One. 19(5):e0302545.
22. You S, Lin S, Feng Y, Fan J, Yan Z, Liu S, *et al*. 2024. ISLS: An illumination-aware sauce-packet leakage segmentation method. Sensors (Basel). 24(10):3216.
23. Juan Z, Zhang J, Gao M. 2024. A multimodal travel route recommendation system leveraging visual transformers and self-attention mechanisms. Front Neurorobot. 18:1439195.
24. Liu X, Song JL, Wang SH, Zhao JW, Chen YQ. 2017. Learning to diagnose cirrhosis with liver capsule guided ultrasound image classification. Sensors (Basel). 17(1):149.
25. Klauder JR, Fantoni R. 2024. The secret to fixing incorrect canonical quantizations. Academia Quantum. 1(1):7349.
26. Byra M, Styczynski G, Szmigielski C, Kalinowski P, Michałowski Ł, Paluszkiewicz R, *et al*. 2018. Transfer learning with deep convolutional neural network for liver steatosis assessment in ultrasound images. Int J Comput Assist Radiol Surg. 13(12):1895-1903.
27. Brattain LJ, Telfer BA, Dhyani M, Grajo JR, Samir AE. 2018. Objective liver fibrosis estimation from shear wave Elastography. Annu Int Conf IEEE Eng Med Biol Soc. 2018:1-5.
28. Yu Y, Wang J, Ng CW, Ma Y, Mo S, Fong ELS, *et al*. 2018. Deep learning enables automated scoring of liver fibrosis stages. Sci Rep. 8(1):16016.
29. Wang K, Lu X, Zhou H, Gao Y, Zheng J, Tong M, *et al*. 2019. Deep learning radiomics of shear wave elastography significantly improved diagnostic performance for assessing liver fibrosis in chronic hepatitis B: A prospective multicentre study. Gut. 68:729–741.